Transfer of spectral weight in the degenerate Hubbard Model in infinite dimension

Pierre Lombardo and Gilbert Albinet
Laboratoire Matériaux et Microélectronique de Provence associé au Centre National de la Recherche Scientifique, UMR 6137, 49, rue Joliot Curie BP, 146, 13384 Marseille Cedex 13, France

(Received 12 December 2000; revised manuscript received 27 August 2001; published 28 February 2002)

Infinite dimensional degenerated Hubbard model has been studied within the framework of the generalized noncrossing approximation. Details on the behavior of excitation spectra are given here, concerning transfer of spectral weight between different energy scales as well as low energy excitation properties. Effective mass evolution close to metal-insulator transitions has been investigated.

DOI: 10.1103/PhysRevB.65.115110 PACS number(s): 71.10.Fd, 71.27.+a, 71.30.+h, 71.28.+d

I. INTRODUCTION

Recent research concerning high-temperature superconductors[1] and giant magneto-resistance[2] have stimulated the interest for strongly correlated electronic systems. Despite a large amount of papers on this fascinating field, a complete physical understanding of these systems remains a major problem of condensed matter theory. Even the simplest Hamiltonian describing such systems, given by the Hubbard model, is still an unsolved challenging problem.

The seminal work of Metzner and Vollhardt[3] has shown the importance of large spatial dimensions D. Taking the limit $D\rightarrow\infty$ leads to significant simplification of the many body problem while retaining essential dynamical features of low dimensional situations. An important amount of studies has been done within this approach, mapping the lattice problem onto a self-consistent Anderson single impurity model. This mapping becomes exact in the limit of infinite spatial dimension. For a review, see Ref. 4. Most of this work has been done focusing on the original one-band Hubbard model, which is the simplest model to describe the electron-electron interaction-driven metal-insulator transition (MIT).

However, orbital degeneracy is known to play a crucial role in correlated systems. The degeneracy of the d band is two in V_2O_3 (Ref. 5) and three in $LaTiO_3$. Orbital degree of freedom is relevant to explain some very interesting properties like colossal magnetoresistance,[6] MIT in alkali-doped fullerenes,[7,8] and for any physical property involving orbital ordering.

Many theoretical approaches have been proposed to describe the effect of strong Coulomb interaction in systems with orbital degeneracy, using the slave-boson method,[9–12] the variational method,[13] and the limit of high spatial dimension. Some results of these works concerning the transition criteria and the order of the MIT are substantially different. A unified theory describing degenerate Hubbard model is still missing. Concerning high spatial dimension approaches, quantum Monte-Carlo (QMC) (Refs. 14,24) and a generalized iterated perturbation theory (IPT) (Ref. 15) have been proposed. Imaginary time results, high computational time and fundamental difficulties at low temperature can be a limit for QMC calculations. The generalization of the IPT, developed in Ref. 16, presents the advantage of being able to deal with particle-hole asymmetric problems. However, this approach is essentially a perturbation theory with respect to the correlation strength, which is the highest energy scale of the system. The noncrossing approximation (NCA) (Ref. 17) was shown to be in excellent agreement with quantum Monte Carlo calculations for the dynamical mean field theory (DMFT) of the one-orbital case,[18,19] even far away from half-filling. NCA has also been used successfully for multichannel impurity models.[20] Here, we present an approach based on the NCA within the dynamical mean field DMFT.

II. THEORY

We start with the standard two-orbitals degenerate Hubbard model taking into account itineracy, strong correlation and two orbitals degree of freedom.

$$H=\sum_{\langle i,j\rangle,a,b,\sigma} t_{ij}^{ab} c_{ia\sigma}^{+} c_{jb\sigma} + \frac{U+J}{2}\sum_{i,a,\sigma} n_{ia\sigma} n_{ia-\sigma} + \frac{U}{2}\sum_{i,a\neq b,\sigma} n_{ia\sigma} n_{ib-\sigma} + \frac{U-J}{2}\sum_{i,a\neq b,\sigma} n_{ia\sigma} n_{ib\sigma} - \frac{J}{2}\sum_{i,a\neq b,\sigma} c_{ia\sigma}^{+} c_{ia-\sigma} c_{ib-\sigma}^{+} c_{ib\sigma}, \quad (1)$$

where the sum $\langle i,j\rangle$ is the sum over nearest neighbor sites of a Bethe lattice and $a,b=1,2$ is the band index. $c_{ia\sigma}^{+}$ (respectively, $c_{ia\sigma}$) denotes the creation (respectively, annihilation) operator of an electron at the lattice site i with spin σ and orbital index a and $n_{ia\sigma}$ is the occupation number per spin and per orbital. The onsite Coulomb repulsion U and the exchange parameter J are assumed to be independent of orbital. In addition we will neglect the last term by taking $J=0$ in the Hamiltonian (1) and the hopping between different orbitals $t_{ij}^{ab}=-t\delta_{ab}$. Hund's rule coupling influence will be examined in a future work.

Within such approximations, the Hamiltonian becomes

$$H=-t\sum_{\langle i,j\rangle,a,\sigma} c_{ia\sigma}^{+} c_{ja\sigma} + \frac{U}{2}\sum_{i,a,\sigma} n_{ia\sigma} n_{ia-\sigma} + \frac{U}{2}\sum_{i,a\neq b,\sigma} n_{ia\sigma} n_{ib-\sigma} + \frac{U}{2}\sum_{i,a\neq b,\sigma} n_{ia\sigma} n_{ib\sigma},$$

and can be written simply

$$H=-t\sum_{\langle i,j\rangle,a,\sigma} c^{+}_{ia\sigma}c_{ja\sigma}+\frac{U}{2}\sum_{\substack{i,a,b,\sigma,\sigma'\\(a,\sigma)\neq(b,\sigma')}} n_{ia\sigma}n_{ib\sigma'}. \quad (2)$$

This Hamiltonian was studied previously by quantum Monte-Carlo (QMC) in Ref. 14. Integrating out all fermionic degrees of freedom except for a central site $i=o$ in the action associated with Hamiltonian (2) leads to the single-site effective action

$$S_{\rm eff}=-\int_0^\beta d\tau\int_0^\beta d\tau'\sum_{\sigma,a} c^{+}_{oa\sigma}(\tau)\mathcal{G}^{-1}_{oa}(\tau-\tau')c_{oa\sigma}(\tau')+\frac{U}{2}\int_0^\beta d\tau\Bigg(\sum_{a\sigma} n_{oa\sigma}(\tau)n_{oa-\sigma}(\tau)+\sum_{(a\neq b)} n_{oa}(\tau)n_{ob}(\tau)\Bigg),$$

where

$$n_{oa}=n_{oa\uparrow}+n_{oa\downarrow}.$$

Therefore, as in the one-band case, the large-D version of the degenerate two-bands Hubbard model is mapped onto an effective impurity model. The local correlated site is now orbitally degenerated, and two different effective media have to be considered. The corresponding Hamiltonian reads

$$H_{\rm eff}=H_{\rm loc}+H_{\rm med}, \quad (3)$$

where the local part is

$$H_{\rm loc}=\sum_{a\sigma}\varepsilon_o n_{oa\sigma}+\frac{U}{2}\Bigg(\sum_{a\sigma} n_{oa\sigma}n_{oa-\sigma}+\sum_{(a\neq b)} n_{oa}n_{ob}\Bigg),$$

and the coupling with the effective medium is

$$H_{\rm med}=\sum_{\vec{k}a\sigma}(W^a_{\vec{k}}b^{+}_{a\vec{k}\sigma}c_{oa\sigma}+{\rm H.c.})+\sum_{\vec{k}a\sigma}\varepsilon^a_{\vec{k}}b^{+}_{a\vec{k}\sigma}b_{a\vec{k}\sigma}.$$

ε_o is the onsite energy for the impurity site. $W^a_{\vec{k}}$ represents hybridization between the site $i=o$ and the effective medium corresponding to a orbital. $\varepsilon^a_{\vec{k}}$ is the band energy of the same effective medium. $b^{+}_{a\vec{k}\sigma}$ (respectively, $b_{a\vec{k}\sigma}$) is the creation (respectively, annihilation) operator of an electron in the a effective medium. The orbital dependent coupling with this two-components effective medium is characterized by the following effective dynamical hybridizations:

$$\mathcal{J}^a(\omega)=\sum_{\vec{k}}\frac{|W^a_{\vec{k}}|^2}{\omega+i0^+-\varepsilon^a_{\vec{k}}}.$$

From the equation of motion of the local Hamiltonian (3), it follows that

$$G_{a\sigma}(\omega)^{-1}=\omega-\varepsilon_o-\Sigma_{a\sigma}(\omega)-\mathcal{J}^a(\omega).$$

Comparing this equation to the following property of Green's functions on a Bethe lattice

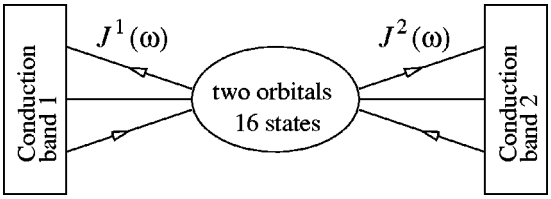

FIG. 1. Two orbitals local model. The sixteen local states $|\alpha,\beta\rangle$ are all coupled by the orbital dependent effective medium hybridization $\mathcal{J}^1(\omega)$ and $\mathcal{J}^2(\omega)$.

$$G_{a\sigma}(\omega)^{-1}=\omega-\varepsilon_o-\Sigma_{a\sigma}(\omega)-t^2G_{a\sigma}(\omega),$$

we found the self-consistent set of equations

$$\mathcal{J}^a(\omega)=t^2G_{a\sigma}(\omega).$$

In the following, we solve the impurity model of Eq. (3) using the extended version of the noncrossing approximation presented in a previous work.[22] NCA is a perturbative approach with respect to the hybridization of the impurity with the effective bath. Therefore, NCA is a good approximation for large values of U. Propagators and self-energies of the sixteen local states $|\alpha,\beta\rangle$ are introduced, where α (respectively, β) is the local occupation of orbital $a=1$ (respectively, $a=2$). Each local state $|\alpha,\beta\rangle$ is an eigenstate of the local part of the model Hamiltonian. The corresponding local model that have to be solved is schematically represented in Fig. 1. The impurity site is coupled with two effective media by two effective dynamical hybridizations $\mathcal{J}^1(\omega)$ and $\mathcal{J}^2(\omega)$.

Local states $|\alpha,\beta\rangle$ and $|\alpha',\beta'\rangle$ are coupled by NCA equations if one of the two following conditions is fulfilled: $\{|n_{o1}(\alpha)-n_{o1}(\alpha')|=1$ and $\beta=\beta'\}$ or $\{\alpha=\alpha'$ and $|n_{o2}(\beta)-n_{o2}(\beta')|=1\}$ as shown in Fig. 2. The first (respectively the second) case involves $\mathcal{J}^1(\omega)$ [respectively, $\mathcal{J}^2(\omega)$].

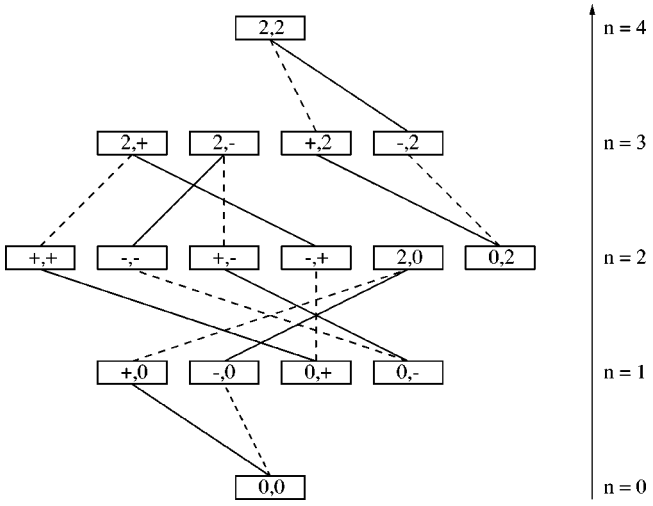

FIG. 2. NCA coupling between the sixteen local eigenstates of the local part of Hamiltonian (3). Only coupling involving the $a=1$ effective medium are displayed. Solid line (respectively, dashed line) represents coupling by exchanging an electron of spin up (respectively, of spin down).

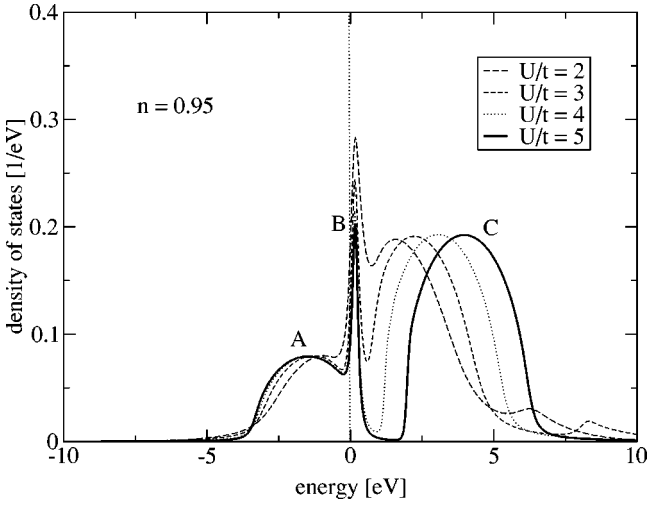

FIG. 3. Densities of states for a constant electronic occupation $n=0.95$ and for various interaction strength $U/t=2$, 3, 4, and 5.

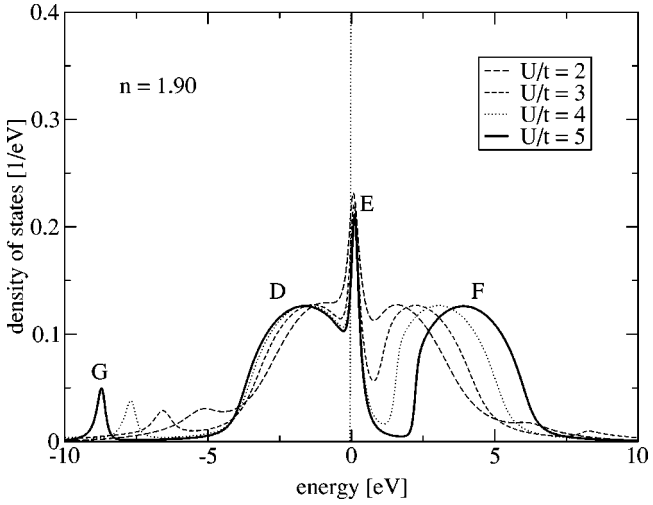

FIG. 4. Densities of states for a constant electronic occupation $n=1.90$ and for various interaction strength $U/t=2$, 3, 4, and 5.

NCA was in very good agreement with essentially exact quantum Monte Carlo simulations for the one-band case. This approximation is then a good candidate for the investigation of the multiband generalization of the Hubbard model. In the next section we present the main results of our dynamical mean field theory.

III. RESULTS AND DISCUSSION

A. Density of states

The NCA approach presents the advantage to provide directly real frequencies one-particle Green's functions. Local quantities like densities of states can therefore be computed for any regime of parameters without having to perform analytical continuation. Useful and comprehensive information concerning electronic dynamic processes are given by these densities of states, without any size effects due to small clusters and till very low temperature. Nevertheless, temperature has to remain higher than a critical temperature under which the NCA presents a pathological behavior. We will discuss this point in the following of the paper.

Spin and orbital dependent densities of states $\rho_{a\sigma}(\omega)$ are obtained from NCA Green's functions by

$$\rho_{a\sigma}(\omega)=-\frac{1}{\pi}\mathrm{Im}\{G_{a\sigma}(\omega)\}.$$

A typical NCA density of states per spin and per orbital is displayed in Fig. 3 for the doubly degenerate Hubbard model and for a total occupation number around $n=1$. Both lower [LHB, (A)] and upper [UHB, (C)] Hubbard bands are present. As in the one orbital case, these high energy excitations are separated by energy U. Relative spectral weights between LHB and UHB are given by the ratio 1/3. Quasiparticle excitations can be seen around the Fermi level [band (B)]. The origin of this low energy structure can be clarified in the context of NCA by observing its temperature and filling dependence[19] or by reducing the Hilbert space of available local states onto the impurity.[22]

The temperature dependence of low energy excitations will be examined at the end of this section. For all other calculations of this paper, temperature has been chosen high enough ($T=1000$ K) to prevent from the NCA pathology at low temperature. The critical temperature for this NCA pathology is around $T=250$ K.[19,21]

The evolution of electronic densities of states with respect to correlation strength U/t is shown in Fig. 3 for an almost quarter-filled system, and in Fig. 4 for an almost half-filled one. $n\approx 1$ in Fig. 3 and $n\approx 2$ in Fig. 4. We do not consider exactly half- and quarter-filled systems to prevent numerical problems from arising when the Fermi level density of states is very close to zero. Nevertheless, our approach is numerically well defined for filling arbitrary close to integer values, with increasing numerical efforts. As in the one-orbital metal to insulator Mott transition, an increasing U/t produce an important transfer of spectral weight from low to high energy scale. Low energy excitations get narrower and Hubbard bands appear simultaneously. Lower and upper Hubbard bands positions are shifted by an energy of order U. Contrasting with these common properties, quarter-filled and half-filled systems differ strongly regarding the spectral weight distribution between occupied and empty states. For large values of U/t where LHB and UHB are well separated, relative spectral weight is 1/3 for $n=1$ and 2/2 for $n=2$. The $n=2$ electron-hole symmetry is no more fulfilled for $n=1$. In this paper, we will examine in detail the doping dependent transfer of spectral weight which is responsible for this behavior.

The correlation strength U/t has been chosen large enough to expect that the noncrossing approximation is correct. NCA is a perturbation theory in which the small parameter is the hybridization between the impurity and the conduction bath. This approach has the advantage of taking into account explicitly all many particles local states for the impurity. Thus, the atomic limit where U/t is large is exact. On the other hand, one severe drawback of the NCA is its failure to capture the noninteracting case.

To understand the influence of orbital degeneracy in this

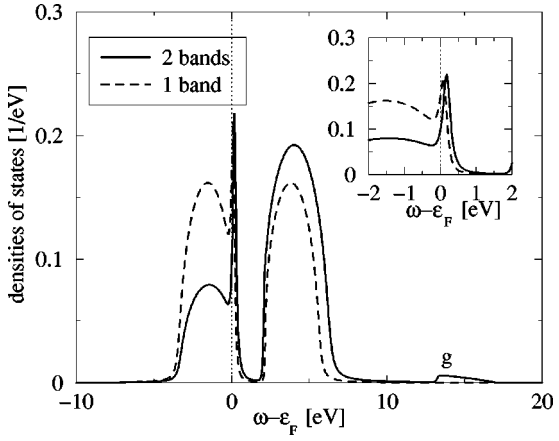

FIG. 5. Comparison of NCA densities of states for a one orbital Hubbard model and for the two degenerate orbitals Hubbard model. Parameters are $U/t=5$ and $n_{\mathrm{tot}}=0.94$ in both cases. The inset shows the low energy behavior of the same densities of states in details. Label (g) designates a band which will be discussed in Sec. III C.

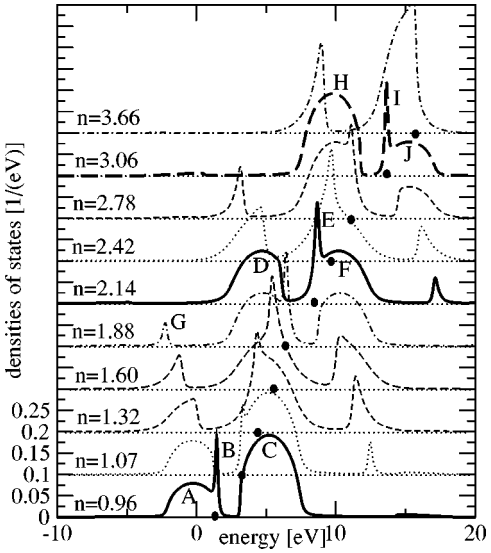

FIG. 6. Densities of states per spin and per orbital for various fillings. The correlation strength is $U=5$ eV, $t=1$ eV and temperature is $T=1000$ K. For each curve, Fermi level is labeled by a black point.

model, it is interesting to compare two-bands densities of states with one-band NCA results. This is shown in Fig. 5, for $U=5$ eV and $n_{\mathrm{tot}}=0.94$. Spectral weights are in good agreement with previous approaches such as IPT.[15] More precisely, we found that degeneracy has a strong influence only on high energy excitations: respective spectral weights of lower and upper Hubbard bands for $n_{\mathrm{tot}}=1$ are 1 and 3 in the two-orbitals problem, instead of 1 and 1 for the same filling in the one-orbital problem. However, NCA band structures are strongly different from IPT ones. Fine structures displayed by IPT results are not present in our approach which is confirmed by recently obtained QMC spectral functions for the multiorbital Hubbard model in infinite dimension.[24]

Figure 6 shows the DMFT-NCA densities of states per spin and per orbital for various fillings and for $U=5$ eV, $t=1$ eV, and $T=1000$ K. The temperature is high enough to be far from the NCA pathology at low temperature. In the strongly correlated regime where $U/t=5$, NCA is a good approximation. Each density of states corresponds to a given electronic occupation increasing from 0.96 to 3.66. In order to examine more clearly spectral weight transfers between bands, densities of states have not been displayed with respect to the shifted energy $\omega-\varepsilon_F$ but directly with respect to ω. Therefore, contrasting with other plots in the paper, Fermi level position is not zero. For each curve, Fermi level position is labeled by a black point on the energy axis. Total occupation numbers n are indicated for each density of states. Quasiparticle low energy excitations can be seen around the Fermi level. Qualitative effective mass behavior of quasiparticles can be deduced from the thickness of the low energy excitation peak. Note that effective mass of quasiparticles increases when approaching the Mott insulating state, which is consistent with experimental observations in filling controlled oxides family such as $Sr_{1-x}La_xTiO_3$.[23] A quantitative study of the quasiparticle effective mass will be done in Sec. III C. For integer fillings $n=1$, $n=2$, and $n=3$, the system is an insulator. It is metallic for any other filling. This is in good agreement with the metal-insulator phase diagram obtained by Quantum Monte Carlo simulations in Ref. 14. For $n=0.96$ the system is metallic. The high effective mass of band (B) quasiparticles is the signature of the proximity of the MIT. High energy bands (A) and (C) display a relative spectral weight which is consistent with probabilities for adding or removing an electron to the system in a singly occupied configuration. Doping up to the intermediate filling $n=1.6$, a complete redistribution of spectral weights is observed. The system is still a metal. A structure is still observed around the Fermi level but the peak is broader. The corresponding effective mass is smaller. The metallic system is far from the insulating phase. Higher energy structures can be well understood by looking at the spectrum evolution for various values of the occupation n. For example, the small spectral weight of band (G) of the $n=1.88$ density of states, can be interpreted as the small probability of removing an electron from a singly occupied site. This probability was large for n close to 1 [band (A)] and strongly decreases for increasing n. For $n\approx 2$, singly occupied sites are unlikely and band (G) spectral weight vanishes. On the contrary the probability of adding an electron onto a doubly occupied site is increasing with n and is represented by the right band (F) in the $n=1.6$ spectrum. Such probability interpretation of densities of states will be detailed in the following of the paper (see Sec. III B).

More information on these metal-insulator transitions can be obtained by plotting the Fermi level dependence of total occupancy. This is displayed in Fig. 7. As it was recently observed by QMC simulations for the multiorbital Hubbard model[24] a plot of occupation number versus chemical potential displays a plateau as soon as a MIT is crossed. When the system in an insulator, as for $U=4$ eV in the figure, a small displacement of the Fermi level in the insulating gap does not lead to a significant variation of the total occupation

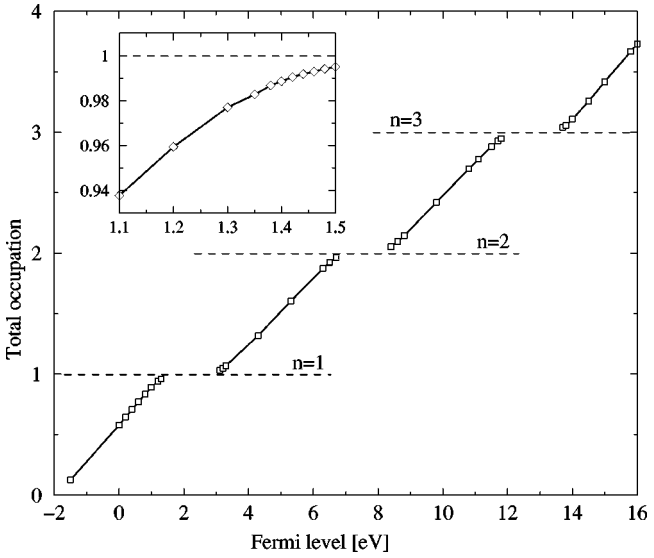

FIG. 7. Total occupation number with respect to Fermi level of d electrons. Parameters are $U=5$ eV, $t=1$ eV and temperature is $T=1000$ K. The inset shows the occupation up to the transition value $n=1$, for $U=4$ eV.

number. Our results show that three successive MIT at integer fillings occur in the system. $n=1$ and $n=3$ transitions are equivalent because of the particle-hole symmetry. For a given U, the Mott gap of the $n=2$ transition is smaller than the $n=1$ gap. This is in good agreement with previous calculations leading to a larger critical U_c for the $n=2$ transition.[14] We found $U_c(n=2)\approx 3.5$ and $U_c(n=1)\approx 3.1$. The inset shows that although an exactly integer value is not possible using NCA because of numerical problems arising from a zero density of states at Fermi level, fillings very close to integer values are nevertheless accessible.

The sequence of MIT for integer fillings is a natural generalization, using Landau theory analysis, of the well known first order MIT for the one-orbital model at half-filling. In a recent work,[25] clear numerical evidences have been given by QMC for the coexistence of metallic and insulating solutions for the DMFT in a half-filled one-orbital Hubbard model at finite temperature. These results are consistent with a finite-temperature numerical renormalization group study of the Mott transition for the same system.[26] The problem of the coexistence of two solutions at integer fillings for the two-orbital model have not been discussed here because of the NCA pathology at low temperature. Indeed, the critical temperature for the NCA pathology is of the order of the temperature at which the coexistence is observed by other approaches. In spite of this shortcoming, our approach has the advantage of providing directly and easily real frequency results.

The transfer of spectral weight upon doping is shown in Fig. 8. Only empty states have been displayed, corresponding to experimental inverse photoemission spectra. The upper part (a) of the figure corresponds to a first domain, where total occupation number goes from $n\approx 0$ to $n\approx 1$ (and empty states number goes from 4 to 3). Starting for the $n\approx 1$ side, where we have three holes per site, and adding holes, Fig.

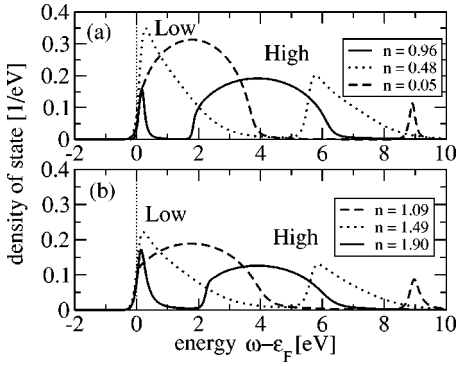

FIG. 8. Unoccupied part of densities of states for various electron fillings. The (a) part of the figure corresponds to total occupations from $n\approx 0$ to $n\approx 1$ (quarter filling) and the (b) part from $n\approx 1$ to $n\approx 2$ (half filling). Parameters are $U/t=5$ and $T=1000$ K.

8(a) shows that added holes go preferentially in low energy states and at the same time, a transfer of spectral weight occurs from high to low energy states. A similar behavior is observed in the second domain [part (b)], where n goes from quarter-filled case $n\approx 1$ to half-filled case $n\approx 2$. Such spectral weight transfers are consistent with expected behavior of strongly correlated systems.

Integrated spectral weight of each unoccupied band with respect to electronic occupation number are displayed in Fig. 9. For electron filling going from $n\approx 2$ to $n\approx 3$ the electron-hole symmetry can be used. Going from $n\approx 2$ to $n\approx 0$, new added holes display the following general behavior previously discussed: new holes go preferentially into states close to the Fermi level and at the same time, an important transfer of spectral weight from high to low energy scale takes place.

The behavior of the low energy part of the spectral weight upon temperature is displayed in Fig. 10. Temperature is chosen such that our results are believed to be not affected by the NCA pathology at very low temperature.[19,21] The states near the Fermi level are strongly temperature dependent. At low temperature, a coherent quasiparticle peak occurs close to the Fermi level. The same kind of behavior was observed for the one orbital system[19] and for the two-band system (transition metal and oxygen).[22] As was already discussed in

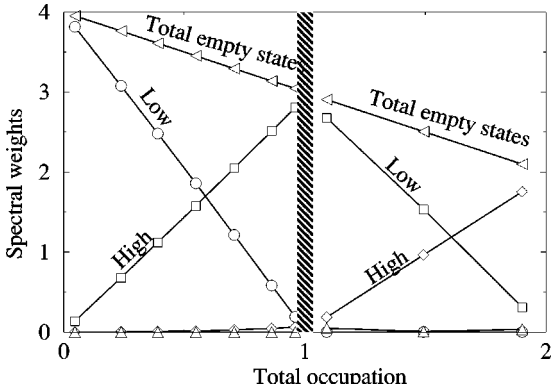

FIG. 9. Integrated spectral weight of each unoccupied band with respect to electronic occupation number. Temperature is $T=1000$ K and $U/t=5$.

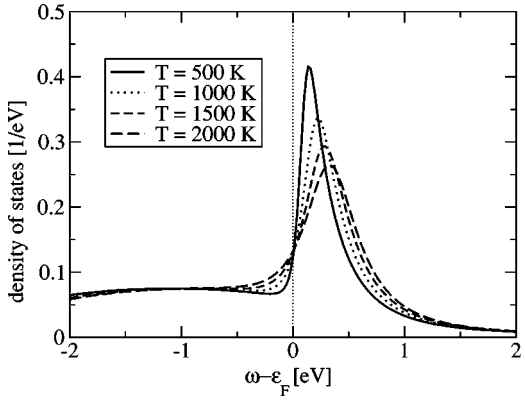

FIG. 10. Densities of states for various temperatures from $T=500$ K to $T=2000$ K. $U/t=5$ and electronic occupation number is $n=0.83$.

Fig. 5 the degeneracy has a strong influence only on high energy excitations.

B. Multiparticle Green's functions

One of the advantages of the DMFT-NCA approach presented in this paper is to provide an easy way for computing various Green's functions. The usual one-particle Green's function $G^a_\sigma(\omega)\equiv\langle\langle c_{a\sigma};c^\dagger_{a\sigma}\rangle\rangle_\omega$ is given by the following expression with respect to the local NCA propagators:

$$G^a_\sigma(\omega)=\sum_{ij}\,(D_{a,\sigma})_{ij}[(D_{a,\sigma})^\dagger]_{ji}\langle\langle X^{ij};X^{ji}\rangle\rangle_\omega,$$

where the projectors X^{ij} are defined by

$$X^{ij}\equiv|i\rangle\langle j|.$$

$\{|i\rangle\}$ are the sixteen eigenstates of the local part of the Hamiltonian (3). The (16×16) matrix $D_{a,\sigma}$ is given by developing the destruction operator $c_{a\sigma}$ on the projector basis $\{X^{ij}\}$:

$$c_{a\sigma}\equiv\sum_{ij}\,(D_{a,\sigma})_{ij}X^{ij}.$$

More complicated Green's functions can be extracted from local propagators $\langle\langle X^{ij};X^{ji}\rangle\rangle_\omega$. Using the same $D_{a,\sigma}$ matrix, two-particles or three-particles Green's functions can be calculated. For example, the useful propagator $F^a_\sigma(\omega)\equiv\langle\langle c_{a\sigma}n_{a,-\sigma};c^\dagger_{a\sigma}\rangle\rangle_\omega$ is given by

$$F^a_\sigma(\omega)=\sum_{ij}\,(\tilde{D}_{a,\sigma})_{ij}[(D_{a,\sigma})^\dagger]_{ji}\langle\langle X^{ij};X^{ji}\rangle\rangle_\omega,$$

where $\tilde{D}_{a,\sigma}$ is the following (16×16) matrix:

$$(\tilde{D}_{a,\sigma})_{ij}=\sum_{kl}\,(D_{a,\sigma})_{ik}(D_{a,-\sigma})_{lk}(D_{a,-\sigma})_{lj}.$$

$F^a_\sigma(\omega)$ Green's function has been recently investigated for the one orbital Hubbard model in Ref. 27.

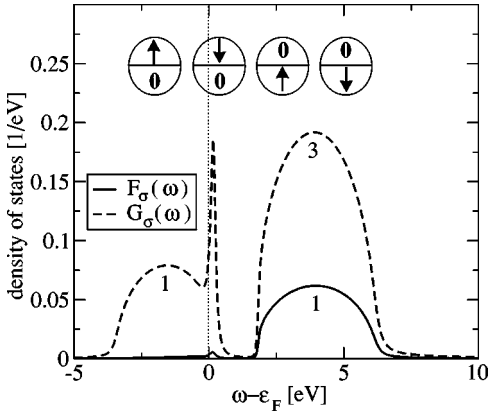

FIG. 11. Spectral densities of $G^a_\sigma(\omega)$ and $F^a_\sigma(\omega)$ for a slightly doped quarter-filled degenerate Hubbard model, for $a=1$ and $\sigma=\uparrow$. Total occupation is $n=0.96$. $U/t=5$ and temperature $T=1000$ K.

Physical interpretation of spectral weight distribution for $G^a_\sigma(\omega)$ function is the following: occupied states spectral weight represents the probability of finding an electron of spin σ in a state of energy ω. Conversely, empty states spectral weight represents the probability, for an extra spin σ electron added to the system, to occupy a state of energy ω. Similar interpretations are valid for $F^a_\sigma(\omega)$ function as soon as one considers the presence of an onsite spin $-\sigma$ electron as an extra necessary condition.

In the following, NCA results for spectral densities of $F^a_\sigma(\omega)$ and $G^a_\sigma(\omega)$ are presented for fillings near quarter-filled case, near half-filled case, and near 3/4-filled case. Figure 11 displays quarter-filled results for propagators as well as most relevant local atomic states. Here we have four such states. In the quarter-filled case, the average number of electron per site is one. Most of the time, a correlated site is singly occupied $|\uparrow,0\rangle$, $|\downarrow,0\rangle$, $|0,\uparrow\rangle$, or $|0,\downarrow\rangle$ depending on the electron spin and on the nature of the occupied orbital. Physical interpretations of $G^a_\sigma(\omega)$ and $F^a_\sigma(\omega)$ spectral densities allow us to explain relative spectral weights of Fig. 11 bands. Concerning $G^a_\sigma(\omega)$, there are three ways (three local states over four) for adding a spin σ electron to the system by $c^\dagger_{a,\sigma}$, and only one way (state $|\sigma,0\rangle$ if $a=1$) for removing an electron by $c_{a,\sigma}$. With the extra condition of having an electron of spin $-\sigma$ on the same orbital, these relative spectral weights become respectively one and zero. This behavior, which is purely due to strong correlations between electrons, is correctly described by the DMFT-NCA.

Corresponding results for the slightly doped half-filled case (respectively, 3/4-filled case) are displayed in Fig. 12 (respectively, in Fig. 13). Calculated behavior for the 3/4-filled case is similar to the quarter-filled case because of the particle-hole symmetry. On the contrary, the half-filled case involves six doubly occupied local states. Removing an electron of spin $\uparrow$ on $a=1$ orbital (applying $c_{1,\uparrow}$) is possible on states $|2,0\rangle$, $|\uparrow,\uparrow\rangle$, and $|\uparrow,\downarrow\rangle$. Applying $c^\dagger_{1,\uparrow}$ is possible on states $|0,2\rangle$, $|\downarrow,\uparrow\rangle$, and $|\downarrow,\downarrow\rangle$. We have therefore equal spectral weights for empty and occupied bands of $G^1_\uparrow(\omega)$ spectral density. With condition $n_{1,\downarrow}=1$, remaining states become

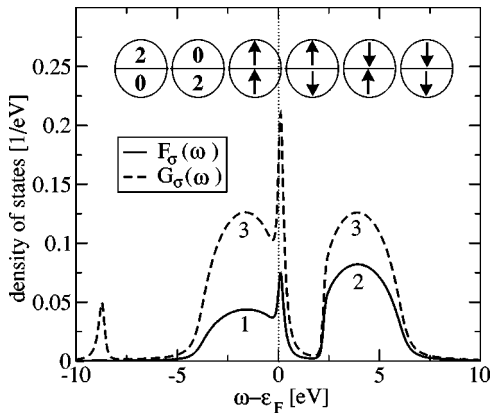

FIG. 12. Spectral densities of $G^a_\sigma(\omega)$ and $F^a_\sigma(\omega)$ Green's functions for a slightly doped half-filled degenerate Hubbard model, for $a=1$ and $\sigma=\uparrow$. Total occupation is $n=1.90$. $U/t=5$ and temperature $T=1000$ K.

only $|2,0\rangle$ for removing one electron, and $(|\downarrow,\uparrow\rangle,|\downarrow,\downarrow\rangle)$ for adding one electron. Calculated results for spectral weights are in good agreement with this qualitative behavior. Relevant microscopic processes between local states can then be identified for each metal-insulator transition.

C. Effective mass

In this section, we present quasiparticle effective masses calculated by NCA for the doubly degenerate Hubbard model. Effective masses are calculated from the frequency dependence of the self-energy real part using the equation

$$\frac{m^\star}{m}=1-\left[\frac{\partial \mathrm{Re}[\Sigma(\omega)]}{\partial\omega}\right]_{\omega=0}.$$

Within the NCA framework, local states self-energies are directly given from local states propagators (see Ref. 22). On the contrary, total interaction part self-energies $\Sigma^U_{a,\sigma}(\omega)$ are calculated indirectly, using the total Green's function

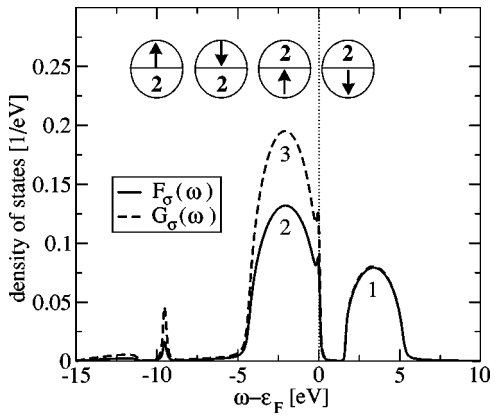

FIG. 13. Spectral densities of $G^a_\sigma(\omega)$ and $F^a_\sigma(\omega)$ Green's functions for a slightly doped 3/4-filled degenerate Hubbard model, for $a=1$ and $\sigma=\uparrow$. Total occupation is $n=2.97$. $U/t=5$ and temperature $T=1000$ K.

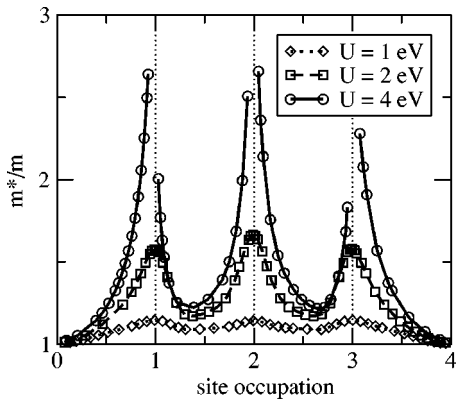

FIG. 14. Doping dependence of quasiparticle effective mass for $T=1000$ K. $U=1$ eV (respectively, $U=2$ eV and $U=4$ eV) is represented by dotted line (respectively, dashed line and solid line).

$$\Sigma^U_{a,\sigma}(\omega)=[G^o_{a,\sigma}(\omega)]^{-1}-[G_{a,\sigma}(\omega)]^{-1}, \tag{4}$$

where

$$[G^o_{a,\sigma}(\omega)]^{-1}=\omega-\varepsilon_o-\mathcal{J}^a(\omega).$$

An alternative way for computing $\Sigma^U_{a,\sigma}(\omega)$ is to estimate the ratio $F^a_\sigma(\omega)/G^a_\sigma(\omega)$:[27]

$$\Sigma^U_{a,\sigma}(\omega)=U\frac{F^a_\sigma(\omega)}{G^a_\sigma(\omega)}. \tag{5}$$

One advantage for using Eq. (5) instead of Eq. (4) is to give a solution for a shortcoming of NCA. NCA is a perturbative approach with respect to the hybridization of the impurity with the effective bath. This implies that NCA can capture many particle dynamical processes which is not possible using a U-perturbative approach. But the noncorrelated situation is not well described by NCA, because hybridization is no more the smallest energy scale in the system. One sign of this important NCA misleading in the $U=0$ case is the calculated density of states which is not identical to the noncorrelated density of states. Therefore $\Sigma^{U=0}_{a,\sigma}(\omega)$ is nonzero when computed by Eq. (4). Using Eq. (5) gives the correct $\Sigma^{U=0}_{a,\sigma}(\omega)=0$.

Figure 14 shows the quasiparticle effective mass behavior with respect to the number of charge carriers per site. For a correlation strength U larger than the Mott transition critical value, divergencies of m^*/m are observed for each integer filling. For smaller values of U, a sensible increase of the effective mass close to integer fillings is precursor to the transition. A strong asymmetry is observed around the $n=1$ and $n=3$ situation contrasting with the particle-hole symmetric case $n=2$. A similar behavior was displayed by a previous QMC approach.[14]

Useful information to understand these properties of symmetry can be obtained within our NCA approach, by comparing densities of states around $n=1$ and $n=2$. Slightly electron-doped and hole-doped situations are displayed in Fig. 15 for $U=4$ eV and $T=1000$ K. Part (a) of the figure corresponds to $n=2$. Corresponding densities of states for electron and hole doped cases are characteristic of a particle-

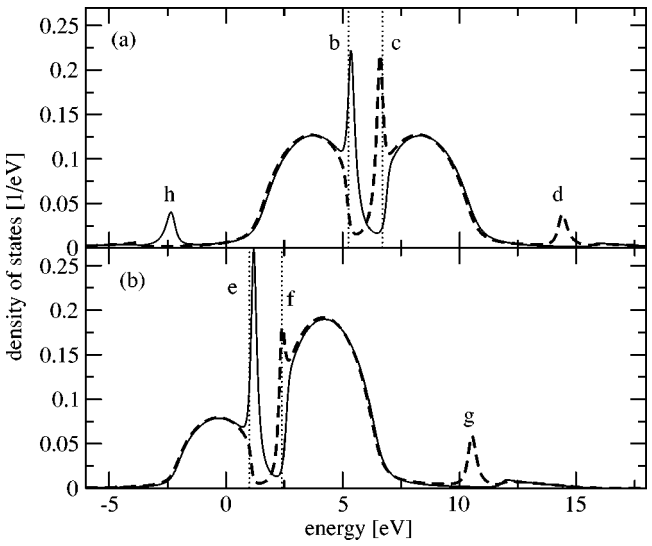

FIG. 15. Densities of states around $n=2$ [part (a)] and $n=1$ [part (b)] for $U=4$ eV and $T=1000$ K. Dotted lines correspond to Fermi levels. Solid line (respectively, dashed line) represents a slightly hole doped (respectively, electron doped) system.

hole symmetric system. For the hole doped system, band (h) corresponds to a nonzero probability of removing an electron onto a singly occupied state. For the electron doped system, band (d) corresponds to a nonzero probability of adding an electron onto a triply occupied state. This symmetric situation is no more valid around $n=1$ (or $n=3$). Band (g) corresponds to a nonzero probability of adding an electron onto a doubly occupied site and does not have any equivalent in the unoccupied part of the spectrum. Indeed, it is impossible to remove an electron from an empty state. Additional bands (h), (d), and (g) are specific to the two-orbitals Hubbard model as shown in Fig. 5. These simple considerations appear directly in the densities of states of Fig. 15, providing a clear interpretation of the relevant electronic dynamics around each metal-insulator transition at integer fillings.

IV. CONCLUSION

In summary, we have proposed an approach based on the dynamical mean field theory for the doubly degenerate Hubbard model, combined with a generalization of the noncrossing approximation in order to solve the equivalent self-consistent local impurity problem. This impurity problem consists in a doubly degenerate local correlated site (sixteen local states) embedded in a conduction band which is orbital dependent.

We obtained a description of the integer filling metal insulator transitions consistent with previous theoretical works using slave-boson formalism,[9–12] variational method,[13] and quantum Monte Carlo dynamical mean field theory.[14,24] The range of validity of our approach is restricted by two important limitations. First, the NCA pathology at low temperature makes it impossible to investigate electronic systems at temperature lower than a critical temperature $T_c \approx 250$ K. This limitation prevents us from discussing the interesting question of the coexistence of two solutions for the MIT at low temperature. Secondly, the exact limit of the NCA is the atomic limit. Therefore, the noncorrelated limit is wrong in this approximation. Despite these limitations, one of the advantages of our approach is to provide the full spectrum of excitations for any value of the occupation number. The effect of orbital degeneracy in density driven Mott transition systems has been studied within this approach. For each metal-insulator transition, relevant microscopic processes have been exhibited. Transfer of spectral weight between different bands have been studied in detail.

In addition, many extensions of the model Hamiltonian can be done within this framework. In future calculations, we will increase the degeneracy (some oxides, like $Sr_{1-x}La_xTiO_3$ are triply degenerate) and we will take explicitly into account the exchange interaction by introducing a nonzero Hund coupling parameter J. The latter is an open question of primary importance as pointed out recently in Ref. 28.

[1] J.G. Bednorz, and K.A. Muller, Z. Phys. B: Condens. Matter **64**, 189 (1986).
[2] R. von Helmolt, J. Wecker, B. Holzapfel, L. Schultz, and K. Samwer, Phys. Rev. Lett. **71**, 2331 (1993).
[3] W. Metzner and D. Vollhardt, Phys. Rev. Lett. **62**, 324 (1989).
[4] A. Georges, G. Kotliar, W. Krauth, and M.J. Rozenberg, Rev. Mod. Phys. **68**, 13 (1996).
[5] C. Castellani, C.R. Natoli, and J. Ranninger, Phys. Rev. B **18**, 4945 (1978).
[6] A.J. Millis, R. Mueller, and B.I. Shraiman, Phys. Rev. B **54**, 5389 (1996).
[7] J.H. Weaver, J. Phys. Chem. Solids **53**, 1433 (1992).
[8] D.M. Pourier, T.R. Ohno, G.H. Kroll, P.J. Benning, F. Stepniak, J.H. Weaver, L.P.F. Chibante, and R.E. Smalley, Phys. Rev. B **47**, 9870 (1993).
[9] J.P. Lu, Phys. Rev. B **49**, 5687 (1994).
[10] H. Hasegawa, Phys. Rev. B **56**, 1196 (1997).
[11] R. Frésard and G. Kotliar, Phys. Rev. B **56**, 12 909 (1997).
[12] A. Klejnberg and J. Spalek, Phys. Rev. B **57**, 12 041 (1998).
[13] J. Bünemann and W. Weber, Phys. Rev. B **55**, R4011 (1997).
[14] M.J. Rozenberg, Phys. Rev. B **55**, R4855 (1997).
[15] G. Kotliar and H. Kajueter, Phys. Rev. B **54**, 14 221 (1996).
[16] H. Kajueter and G. Kotliar, Phys. Rev. Lett. **77**, 131 (1996).
[17] N.E. Bickers, Rev. Mod. Phys. **59**, 845 (1987).
[18] M. Jarrell and T. Pruschke, Phys. Rev. B **49**, 1458 (1993).
[19] T. Pruschke, D.L. Cox, and M. Jarrell, Phys. Rev. B **47**, 3553 (1993).
[20] Tae-Suk Kim and D.L. Cox, Phys. Rev. B **55**, 12 594 (1997).
[21] E. Müller-Hartmann, Z. Phys. B: Condens. Matter **57**, 281 (1984).
[22] P. Lombardo, J. Schmalian, M. Avignon, and K.H. Bennemann, Phys. Rev. B **54**, 5317 (1996)
[23] Y. Tokura, Y. Taguchi, Y. Okada, Y. Fujishima, T. Arima, K.

Kumagai, and Y. Iye, Phys. Rev. Lett. **70**, 2126 (1993).
[24] J.E. Han, M. Jarrell, and D.L. Cox, Phys. Rev. B **58**, R4199 (1998).
[25] J. Joo and V. Oudovenko, Phys. Rev. B **64**, 193102 (2001).
[26] R. Bulla, T.A. Costi, and D. Vollhardt, Phys. Rev. B **64**, 45 103 (2001).
[27] R. Bulla, A.C. Hewson, and T. Pruschke, J. Phys.: Condens. Matter **10**, 8365 (1998).
[28] K. Held and D. Vollhardt, Eur. Phys. J. B **5**, 473 (1998).